An Experimental Study of the Gravitational Collapse of a Granular Gas

by

Reuben Son
Class of 2008

A thesis submitted to the
faculty of Wesleyan University
in partial fulfillment of the requirements for the
Degree of Bachelor of Arts
with Departmental Honors in Physics

ACKNOWLEDGEMENTS

This work is indebted to a network of people:

to Joanne Denworth and the late Raymond Denworth, whose generosity have made the body of research presented in this document possible;
to Ian Hollander, for his friendship over the years;
to John Perez, whose work has laid down the foundations of my research pursuits;
to my current and past labmates – Dan Blum, Rachel Brown, Pennan Chinnasamy, Thomas Glomann, Shabnam Khalighi-Monfared, Surendra Kunwar, Emmalee Riegler, Wa Susantha Wijesinghe – with whom work has been a pleasure;
to Elaine Saly, for her love and support;
to Mark Shattuck, for his advice and insight;
to my family, for believing in me;
to Greg Voth, for his dedication to his students and to science.

Abstract

We observe a finite time collapse of a granular gas under gravity, in which a collapse shock separates two distinct cooling stages. During the latter of these cooling stages, we find the granular temperature to evolve as a power law with an exponent in the range of 4 to 7. These measurements of the power law exponent are significantly higher than the predicted exponent of 2, which signifies a more rapid decay. This is likely due to a combined effect of frictional interactions (particle-particle and particle-sidewall), drag forces, and the quasi-two-dimensionality of our granular system. Additionally, we find evidence contrary to the claim that gravitational collapse occurs simultaneously across height.

Contents

List of Figures

1 Introduction

A granular gas, composed of inelastic hard spheres, is an instance of a granular flow. The dissipative collisions among its composite particles causes a granular gas to always be out of equilibrium, and in this, a granular gas is fundamentally different from a true gas. However, a granular gas may achieve a non-equilbrium steady state while being externally driven. The steady states of driven granular flows have attracted much attention in the past decades, and the approaches of studying these steady states have drawn from theory (hydrodynamic and kinetic), numerical simulations, and experiment. The existence of shock waves [1, 2, 3], density inversion [4], convection rolls [5], breakdown of the equipartition [6], temperature inversion [7, 8], and phase-change [9] have been some of the interesting phenomena observed and studied with regards to these non-equilibrium steady states.

In the absence of energy input, the granular gas freely evolves to a static crystalline state. In recent years, the dynamics of this collapse has begun to gain greater attention in the field, but the majority of studies have been conducted only in theory and simulation, with the exclusion of gravity [10, 11, 12, 13, 14]. Two recent studies [15, 1] have included considerations of gravity in their numerical systems, but to wit, there have been no experimental studies of the inelastic collapse of a granular gas under gravity. The body of research presented in this thesis has been conducted as an experimental study of precisely this gravitational collapse.

Under the exclusion of gravity and density inhomogeneities, the temperature of the homogeneous cooling state (HCS) is predicted to decay as the following power law: $T(t) = T_0(1 + t/t_0)^{-2}$ [10], where t_0 - a function of number density, particle diameter, and the coefficient of normal restitution - is the cooling time after driving is stopped. This result, referred to in the literature as Haff's Law,

has been the starting point of a widely developed Inelastic Hard Sphere (IHS) model, which allows for density inhomogeneities, but not gravitational forces. In the IHS model, density inhomogeneities are found to emerge in the form of clusters [11]. The phenomenon of clustering occurs when inelastic collisions between particles reduces the local kinetic energy, which effectively reduces the mean-free-path about the collisions. Consequently, faster particles will collide with slower ones more frequently, and thus, clusters will form and aggregate until the entire granular flow has crystallized. Because these clusters form spontaneously, they typically generate deviations in the IHS model from the scaling behavior that characterizes the HCS. However, when gravitational forces are included, spontaneous clustering effects are suppressed, and instead, the density inhomogeneities become gravity-driven. A study by Volfson et al. [15] has recently been conducted on the inhomogeneity introduced by gravity, in which a new scaling behavior has been discovered: $E(t) \sim (t_c - t)^2$. This scaling behavior has been posited to be universal (valid for all heights throughout the granular flow), and valid as $t \to t_c$, but the range in which this scaling behavior is valid is not yet known.

Our experiment, which physically models a 2D granular gas, suggests that the decay of total energy of a granular gas may indeed obey a power law, but we find that the exponent in such a power law is greater than 2. The presence of inter-particle friction, wall-drag, and quasi-two-dimensionality, which are not parameters in [15], may be the source of this deviation. In general, this body of research focuses on the entire temporal scope of a gravitational collapse event, within which we draw particular attention to the collapse shock and the subsequent quasi-static flow that follows.

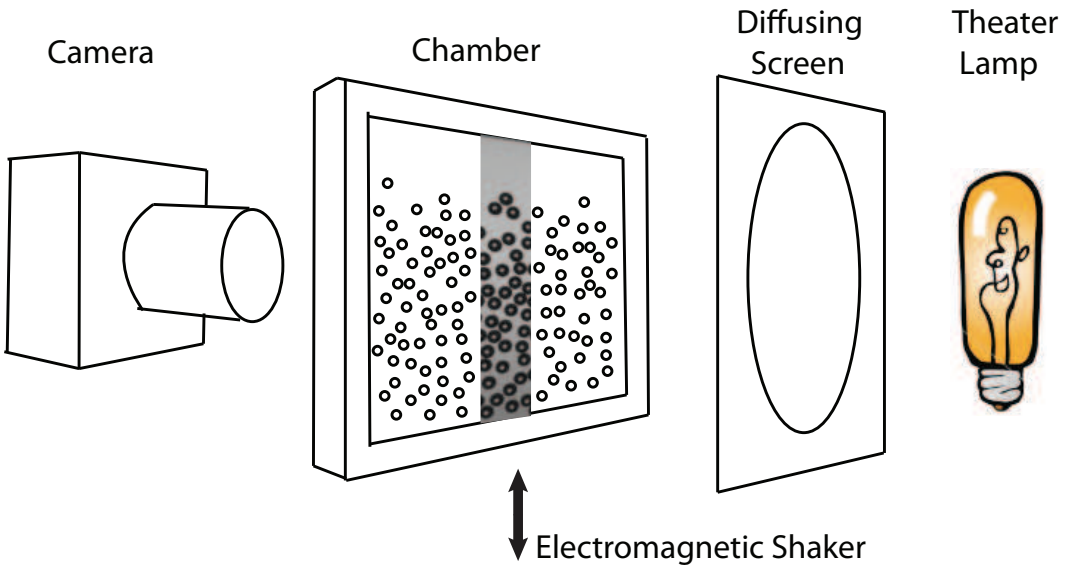

Figure 1: In our experiment, a high-speed video camera captures the motion of spherical particles backlit by a theater lamp. The image placed inside the chamber diagram is an actual instance of our data, and closely represents the region of the chamber we image.

2 Experimental Setup and Procedure

2.1 Experimental Procedure Part I: Data Acquisition

Our granular gas is composed of 285 borosilicate glass spheres of diameter $d =$ 3.175 mm. The coefficients of normal restitution have been previously measured to be $r_{particle-particle} = 0.92$ and $r_{particle-wall} = 0.98$ [16]. The particles are restrained to quasi-two-dimensional space by a chamber apparatus consisting of two glass viewing plates and an aluminum frame. The resulting cell defines a volume measuring 92.3mm x 66.7mm x 3.4mm, or equivalently, 29.07d x 21.01d x 1.07d. In a hexagonally packed static state, the particles sit at 10 monolayers. In this static state, the area fraction occupied by the particles is 0.77, and in a fully fluidized state, the area fraction is 0.37. The chamber, which sits atop an eletromagnetic shaker, is vertically oscillated at 100 Hz for 50 cycles with an amplitude of 870 μm (nondimensional acceleration $\Gamma = 4\pi^2 f^2 A/g = 35$) in order to fully fluidize

the granular gas. Gravitational collapse in the gas is then induced simply by halting the driving force. The halting procedure works by transmitting a transient waveform to the shaker on its downstroke. This waveform has been calculated to optimize the chamber's arrival to its rest position (explained to greater detail in Sec. 2.2).

The temporal scope of the data that we take includes two driving cycles and the entirety of the collapse of the granular gas into a condensed static state. The experiment is centrally controlled and synchronized through a main computer running Labview software. Signals generated in Labview are processed through a digital-analog converter and directed to a high-speed camera and the electromagnetic shaker (Fig. 1). The camera is set up to image only a central strip of the cell, capturing the entire range of the cell height (21d), but limiting the horizontal range of view to 3.65d within the (nearly) horizontally homogeneous region found at the center of the cell. By lowering the image size to 71 x 440 pixels, we optimize the data flow from the camera to the computer, and take images at a framerate of 7000 Hz. The data analyzed in this thesis consists of 1699 identically induced granular collapse events, each consisting of 2200 images (spanning a time of 314 ms).

2.2 Improvements Made to the System

The experimental setup used in conducting this research was developed and built by John Perez ('06) for his doctoral research. During my time working with the system, I have made two modifications. The first was made in an effort to optimize the stopping of the chamber oscillation. Considering our focus on studying the collapse dynamics of a granular gas, it is important to bring the chamber to its rest position as quickly and cleanly as possible. The simplest scenario is that of simply cutting off the sinusoidal signal that drives the shaker. The undesirable

consequence of this approach is that the chamber continues to carry its momentum after the signal disappears, moving in the manner of an under-damped oscillator. The more sophisticated approach - the one employed by John - is to supply to the shaker a transient (Gaussian) signal that briefly drives the chamber upwards on its downstroke. My modification built upon this transient signal and introduced a neglected free parameter, c, in the functional form: $Ae^{-\frac{\omega^2}{2c^2}}$. Through a trial-and-error process of playing with the free parameters and comparing the consequent chamber motions, the chamber-stopping procedure was optimized to have the chamber come completely to rest in the shortest time possible (Fig. 2).

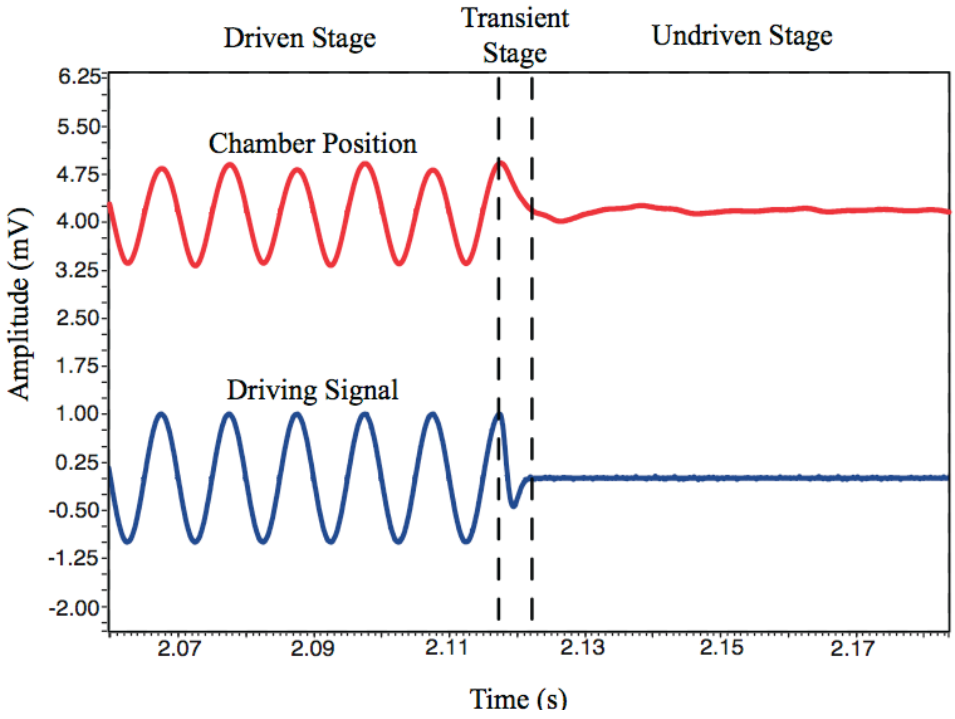

Figure 2: This figure shows the relationship between the signal driving the shaker (blue) and the consequent movement in the chamber (red). The dashed lines demarcate the three functionally separate stages in the operation of the shaker. At the point of the last peak in the driving stage, a transient signal replaces the driving signal. The amplitudes of the signals represented are arbitrary, and it should also be noted that the data presented here for the chamber position have been acquired via a motion sensor, which includes much more noise than we actually see in our data, and has been used here as a matter of convenience.

The second modification to John's setup was made upon the discovery that the chamber was experiencing a low amplitude vibration at 60 Hz during the undriven stage. In the static state, particles were found to be oscillating in unison at 60 Hz at a low enough amplitude ($\Gamma < 1$) that the particles remained still with respect to each other. To confirm that the chamber was indeed vibrating, we looked into the image-recorded motion of the chamber, which we tracked by locating a pixel in each frame containing the boundary between the aluminum frame and the glass plate. In examining the motion of the chamber, we found that the intensity fluctuation of the pixel containing the edge of the aluminum frame had a different waveform than a pixel containing incoming light transmitted directly from the lighting source (Fig. 3a). Using IDL's fft routine, we performed Fourier analysis on the intensity fluctuation of the pixel containing the edge of the aluminum frame (Fig. 3b). The waveform was found to indeed be dominated by a 60 Hz frequency, with a minor contribution at 120 Hz. The 120 Hz frequency corresponds to the light emitted by our light source, and because the pixels cover a 160 μm space that includes both a small glass region (which passes light) and a small aluminum region (which obstructs light), the 60+120 Hz frequency combination corresponds to fluctuations in the ratio of glass-to-aluminum captured in the frame. With the help of Mark Shattuck (CUNY), the origins of the 60 Hz vibration were then located within our setup: the TTL-to-CCD converter used in triggering our camera was found to be relaying a 60 Hz frequency back into our shaker, thus driving it. This undesired driving signal was eliminated by installing an opto-isolator circuit, and as we can see from the corresponding Fourier spectrum (Fig. 3c), the chamber is now free of any undesirable driving force.

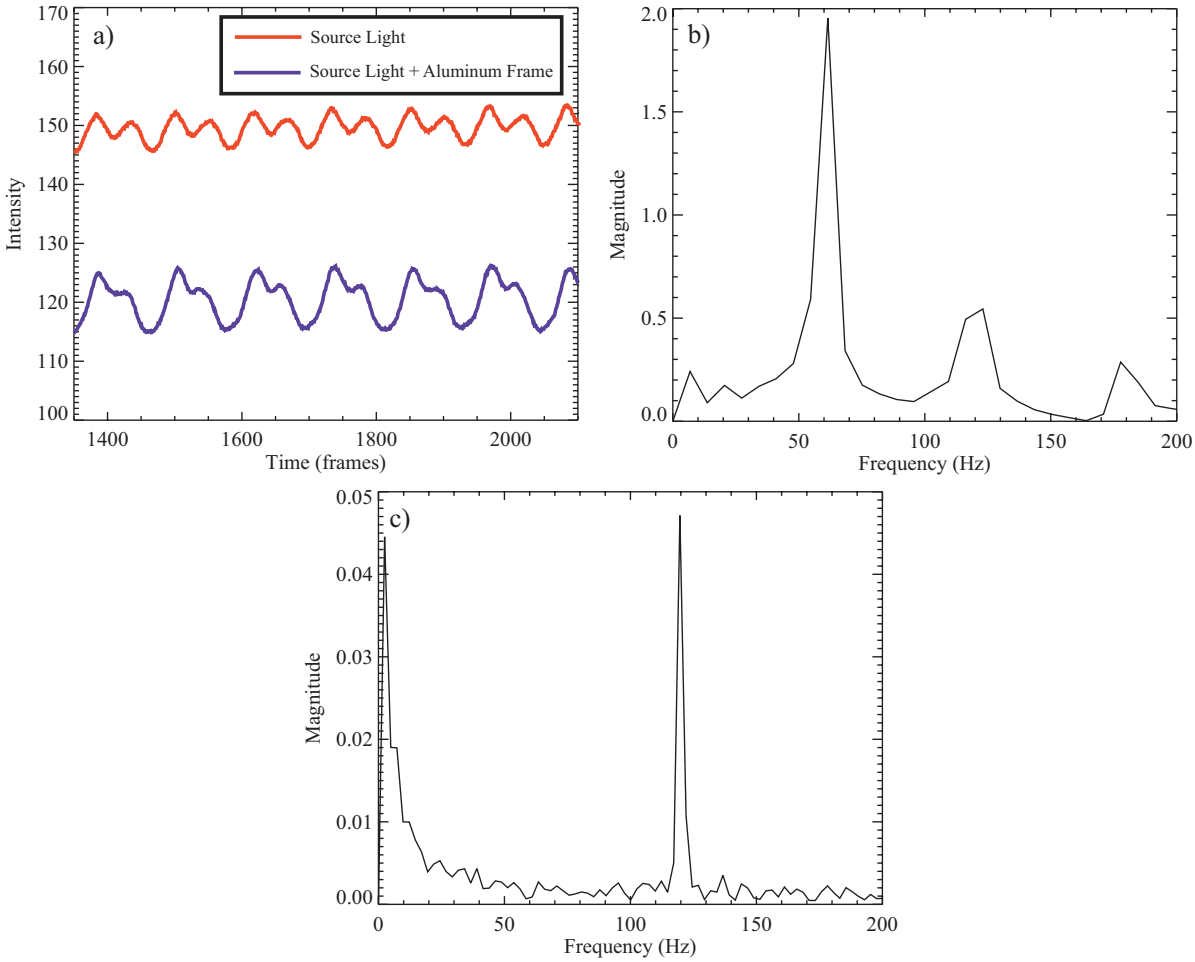

Figure 3: (a) The intensity fluctuations in a pixel containing the edge of the chamber (blue) is plotted against the intensity fluctuations of incoming light. (b) The Fourier spectrum of the waveform reveals its frequency composition to be dominated by a 60 Hz frequency. (c) After installing an opto-isolator to prevent electrical components in our setup from feeding back into the shaker, we see a sharp peak only at 120 Hz, which corresponds to the frequency of light emitted by our light source. The corresponding waveform for c is not depicted.

2.3 Experimental Procedure Part II: Data Processing

From the image data, particle-tracking codes written in IDL extract particle-positions based on the centers of the particles with an accuracy of $\frac{1}{20}^{th}$ of a pixel diameter, or equivalently, $\frac{d}{390}$ or $8.14\,\mu$m. From the particle-positions, particle trajectories are determined, and finally, particle-velocities are measured from the particle trajectories. Because the camera has been framed to image only a central strip of the cell and the system is closed, the horizontal component of the particle-velocities always averages out to zero: $<v_x>=0$. However, the magnitude of the horizontal component of the particle-velocities changes throughout the temporal scope of the experiment. Because the driving force operates only in the vertical direction, the horizontal component of particle velocities emerges only through angular collisions between particles. In regions like the bottom of the cell during the driving stage, where particles experience strong vertical acceleration, $\frac{<|v_x|>}{<|v_y|>}$ is small, but this disproportionality evens out over a number of collisions. This is particularly true as the system moves into the terminally cooling stage close to complete collapse. The disparity between $<|v_x|>$ and $<|v_y|>$ begins to equilibrate as the increasing number of inelastic collisions in all directions overcomes the inhomogeneity introduced by gravity and the driving force. Because $<v_x>$ $=0$ and $<|v_x|>\approx<|v_y|>$ in the cooling range of interest to us, we focus this paper only on the vertical component of particle-positions and velocities. Accordingly, we treat particle-velocities independent of horizontal position, as if our system was one-dimensional. We thus proceed to bin vertical particle-velocities conditioned on height in the chamber and on time-step. By ensemble averaging over 1699 iterations of data acquisition, we effectively sample the single-particle velocity distribution function, $f(y, v_y, t)$, for each time-space bin. From these distributions, we generate the velocity moment fields shown in Figs. 4, 5, 6, and 7. Our bin size of 4 pixels in height and 4 time-steps is sufficiently large to collect

statistics, but small enough at $\approx \frac{d}{5}$ to resolve particle-scale structures.

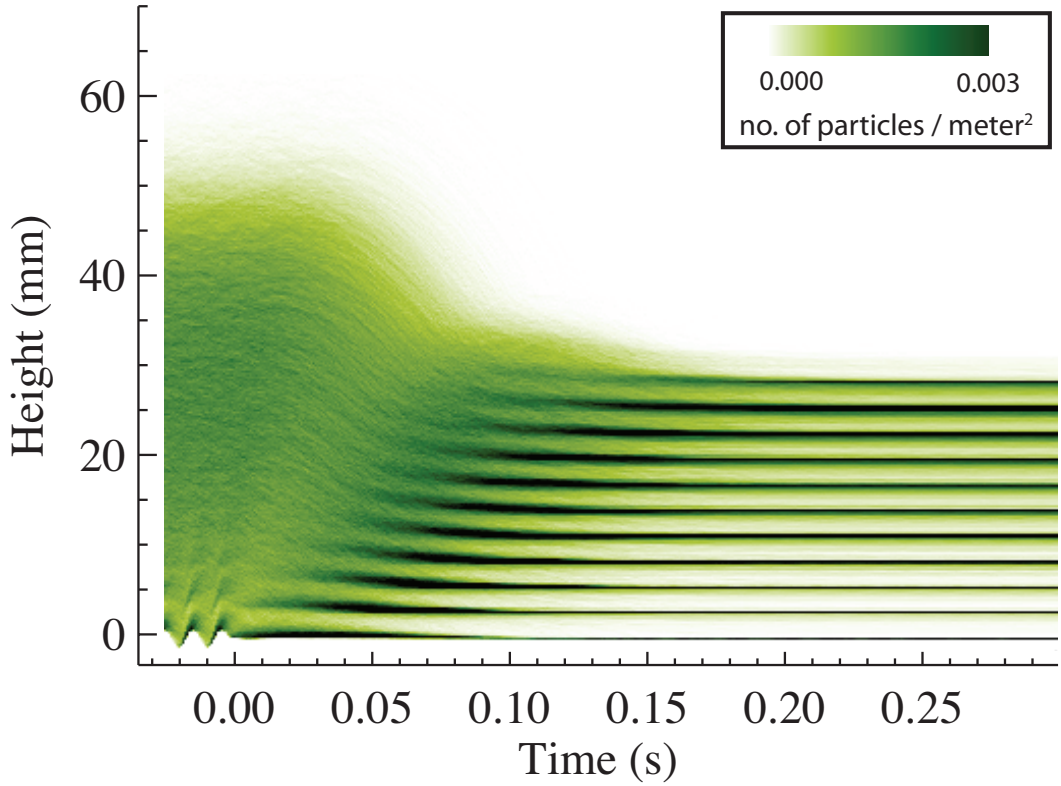

Figure 4: Number density field. In this figure and throughout all the velocity moment fields, the height y=0 is defined to be one particle radius above the actual bottom of the cell in its rest position at $t \geq 0$. At $t < 0$, self-similar density structures originating at the bottom of the cell propagate upwards. The distance of separation between these structures is a measure of the mean free path of the particles driven upwards by the oscillating floor of the cell. The bold horizontal lines in the density profile at times $t > 0.1$ represents the layers that the particles form in their condensed state, and the irregular gradients that emerge between the bold lines represent defects in the crystalline structure. The smallness of our maximum density is the consequence of defining the position of a particle to be its center and the smallness of the bin size.

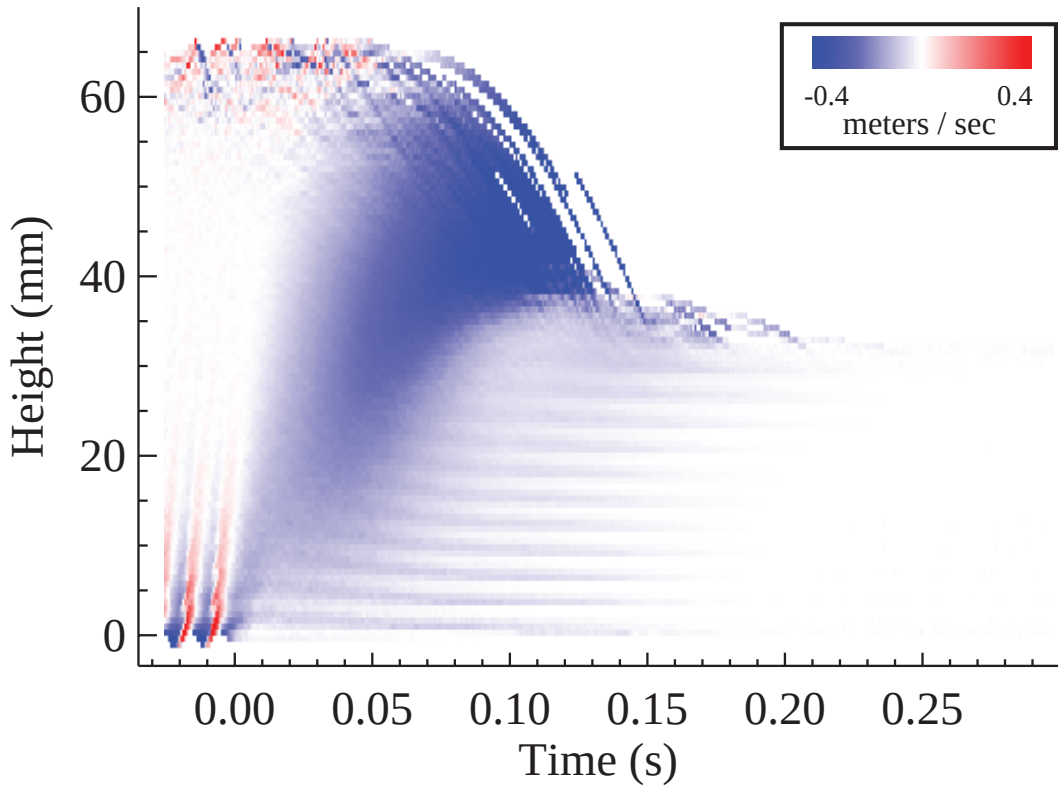

Figure 5: Mean vertical velocity field. At $t < 0$ and $25 < y < 50$, the granular gas is characterized by a mean vertical velocity close to zero. Below this region, shock waves propagate upwards through the momentum transfer between colliding particles, gradually losing magnitude due to the inelasticity of the collisions. The prominent feature of this figure is the negative velocity wave that emerges shortly after gravitational collapse is induced. Following this wave, we see the negative velocities segregate into lines, which correspond physically to the settling of particles into layers.

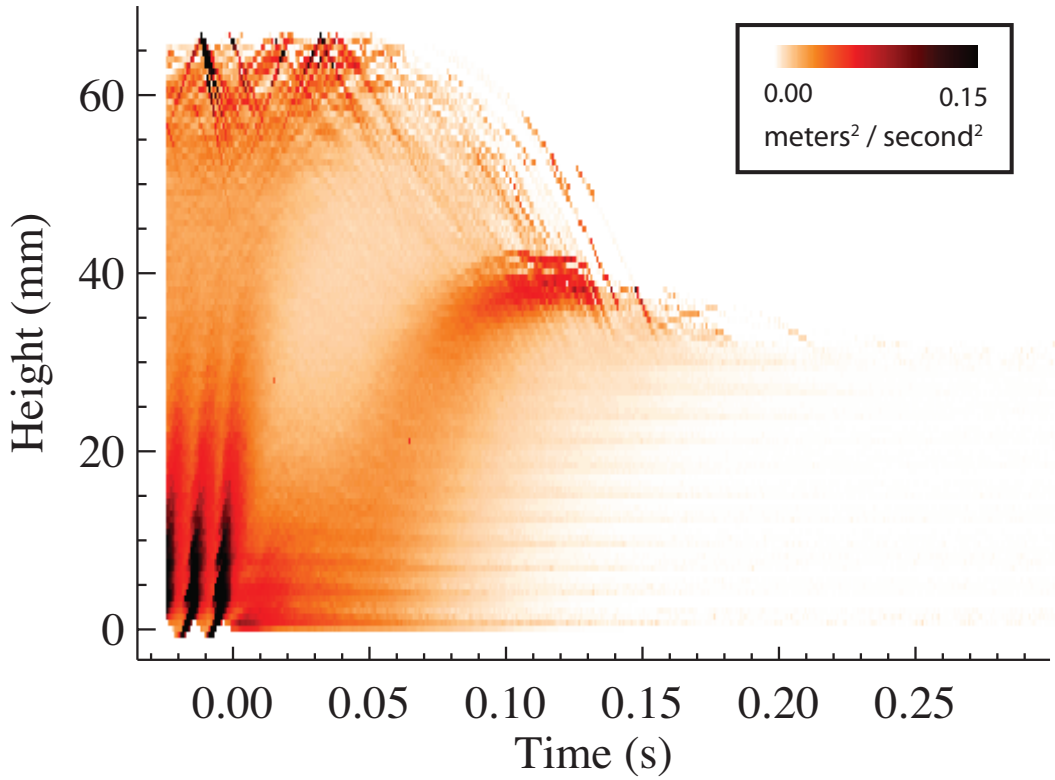

Figure 6: Vertical velocity variance field. After gravitational collapse is induced, much of the granular system experiences a period of free fall, after which a collapse shock propagates upwards from the bottom of the chamber ($t = 0.05$). After the collapse shock, the granular system evolves into a quasi-static flow, in which energy is dissipated through inelastic collisions and frictional interactions until a static state is reached.

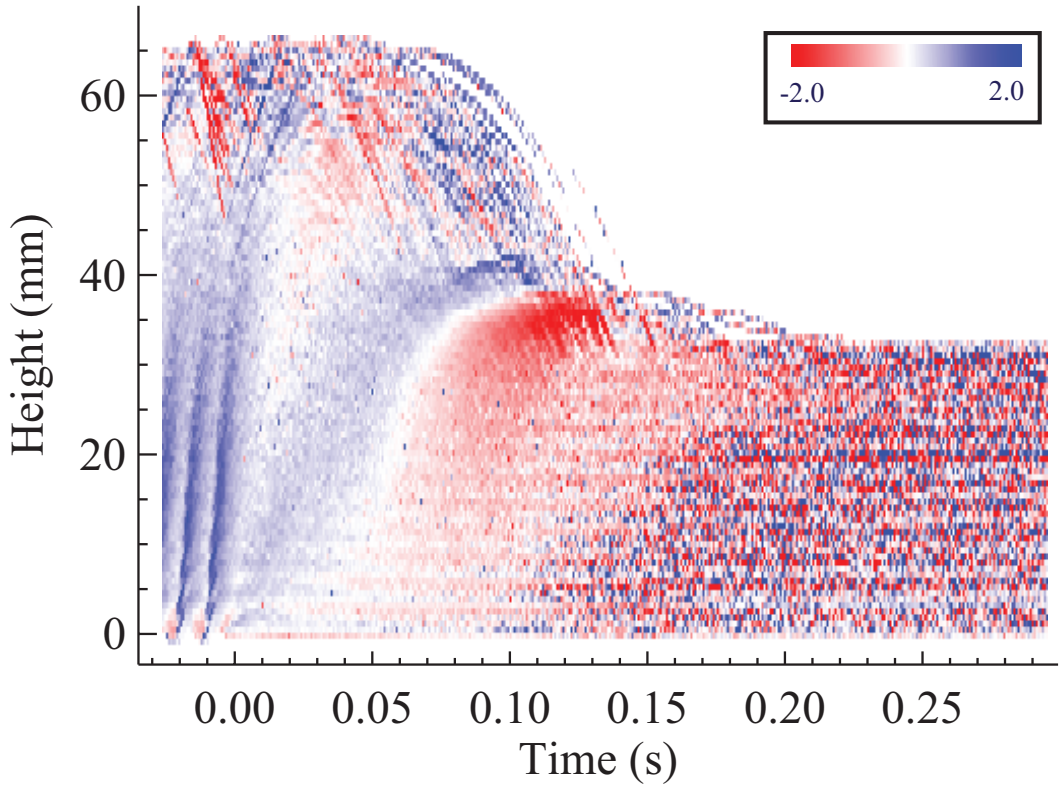

Figure 7: Vertical velocity skewness field. The collisional interactions that comprise the collapse shock are particularly well captured in the sign-disparity towards the center of the figure. The boundary between the region of positive and negative skewness at $0.07 < t < 0.14$ represents the position of the shock wave. About this boundary, positive skewness characterizes the rebounding upward movement of falling particles. Below this boundary, negative skewness characterizes the downward movement of particles which have inherited the momentum of the falling particles. Throughout the figure, we see positive and negative skewness of order 1, which indicates that the velocity distributions are non-Gaussian. This degree of skewness is not sensitive to our bin size.

3 Experimental Results and Discussion

3.1 The Substructure of a Gravitational Collapse

The velocity variance field (Fig. 6) can defined to be a granular temperature field, such that $T(y,t) = <v_y^2> - <\bar{v}_y>^2$, where y and t specify a time-space bin. During both the driven and undriven stages of our data, we see space-time regions

in the temperature field that are fairly homogeneous in themselves, and others that are dominated by inhomogeneous sub-structure. To describe the the local physics of these phenomenologically distinct space-time regions, we deconstruct our temperature field into characteristic collapse regimes (Fig. 8), each of which plays a different role in the space-time evolution of a granular collapse event.

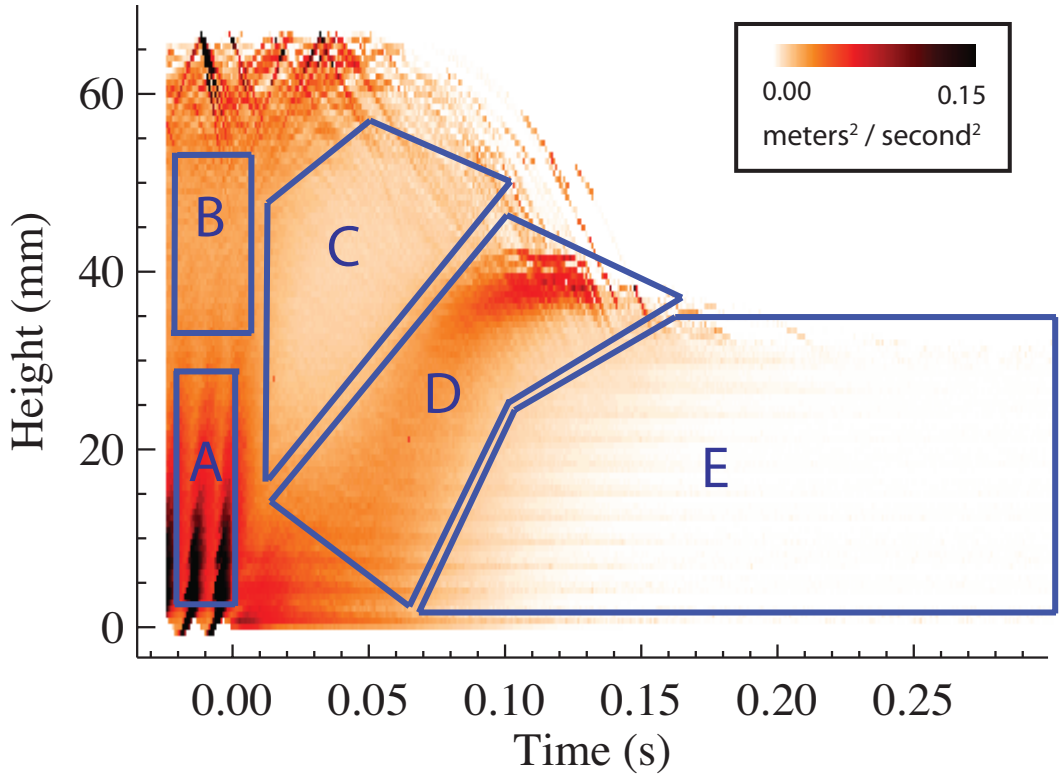

Figure 8: The temperature field of Fig. 6 is reproduced here with the collapse regime demarcations superimposed. Regime A is characterized by an inhomogeneity dominated by shock waves. Regime B is the homogeneous steady-state granular gas. Regime C is the homogeneous freely cooling gas. Regime D is the collapse shock. Regime E is a quasi-static granular flow. The un-demarcated region near $y = 60$ is dominated by rare and violent collisions with the top of the chamber. The un-demarcated region beneath Regime D is characterized by high-energy collisions between the particles above and with the chamber floor below.

In regime A, the gas is characterized by shock waves originating from the bottom of the cell that propagate upwards. As the shock waves travel upwards, the momentum transferred with each collision decreases. Thus, as the magnitude of

the shock waves decreases, the granular temperature becomes more homogeneous and energy is more evenly distributed between the translational and rotational degrees of freedom. In regime B, the time-dependence of temperature disappears and the gas becomes nearly homogeneously fluidized. When the driving force stops, regime B transitions into regime C and the particles begin to pick up negative velocities with gravity while losing energy through inelastic collisions. As the particles of regime C accelerate with gravity, the gas below accumulates in density, and the high-energy confrontation between regime C and the high-density region results in a collapse shock. Through the collapse shock, the freely cooling particles of regime C are deflected back upwards. The mean free path, however, is short in regime D and the majority of particles do not escape this zone of high-energy collisions. The rising density of particles contributes to an accelerated rate of energy dissipation, and thus, high density is propagated through the time evolution of the collapse shock. Following regime D, the granular flow (no longer a granular gas, due to low temperature and high density) becomes characterized by an increasing rate of dissipative collisions, and steadily approaches the static state.

These collapse regimes detail the general phenomenology of a granular collapse event, and in particular, we note that the collapse of the gas involves two cooling stages, separated by a collapse shock. It is in the latter cooling stage that Volfson et al. [15] have proposed that the total translational kinetic energy is dissipated as a power law: $E(t) \sim (t_c - t)^2$ as $t \to t_c$. In order to analyze the collapse time t_c of our own system, we shift over to the Lagrangian mass coordinate, defined $m(y,t) = \frac{1}{N_{total}} \int_0^y N(y',t)\, dy'$, where $N(y,t)$ is the number of particles in a space-time bin and $0 \leq m \leq 1$. By working with this system of non-dimensional mass coordinates, we effectively rescale the mass of our granular gas and gain the advantage of measuring the energy decay of a fluid packet. The limitations

of using Eulerian coordinates is immediately evident when an attempt is made to trace T(y,t) across a fixed height y in Fig. 6, in which case the physics of the traced line would be misleading and difficult to interpret. With the fluid packet approach, a small range, or window, of Lagrangian mass coordinates can be followed through time, which would correspond physically to the statistically probably trajectory of a particle or a number of particles.

3.2 The Global Velocity Variance, $E(t)$

As one can immediately observe in the temperature field (Fig. 6), the notion of global temperature in equilibrium thermodynamics does not apply well to non-equilibrium systems such as ours. However, the global velocity variance can potentially be useful as a measure of the translational kinetic energy, $E(t)$. The time evolution of $E(t)$ in Fig. 9 expresses the key physics previously discussed with regards to the collapse regimes C, D, and E. For $0 < t < 0.02$, the energy drops off as the cooling gas of Regime C freely falls. From $0.02 < t < 0.06$, a rising trend in $E(t)$ represents the high-temperature region associated with the collapse shock. And finally, for $t > 0.06$, the energy goes to zero as the granular flow crystallizes and kinetic energy is transferred to heat. The fundamental conclusion we draw from the time evolution of $E(t)$ is that the energy does not decrease monotonically after collapse is induced ($t \geq 0$). Instead, there is a well-defined bump in the energy that corresponds to the collapse shock, after which the energy monotonically decreases.

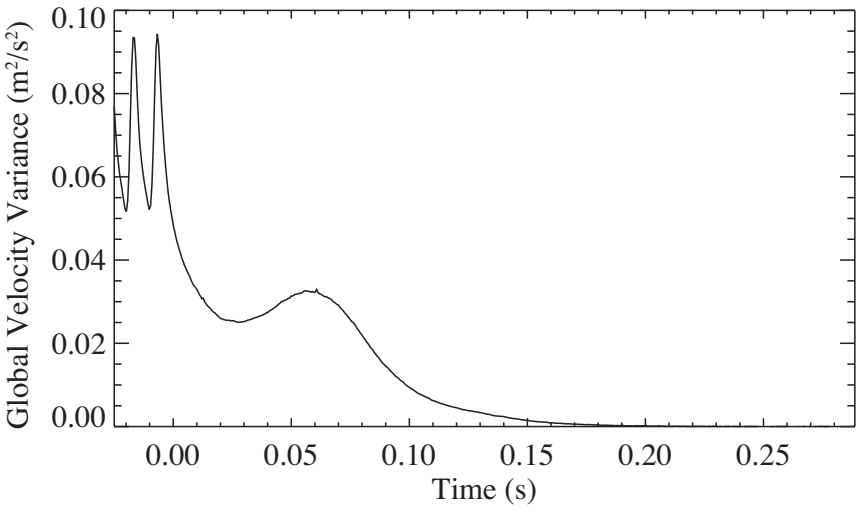

Figure 9: The time evolution of global vertical velocity variance, over all mass coordinates. $t = 0$ has been defined to be the time at which the driving force was halted. The time axis contains the entirety of the temporal scope of our data. Additionally, our calculations of $E(t)$ asymptotically approach $6.2 * 10^{-4}$, which has been subtracted off as noise in this figure. Noise will be similarly subtracted off future figures depicting the time evolution of velocity variance.

3.3 Asynchronicity of Gravitational Collapse

In order to make contact with the prediction of a power 2 decay suggested by simulation and hydrodynamic theory [15], we investigate our measurements of $E(t)$ for evidence of such a scaling behavior. With a non-linear fitting routine based on the functional form $E = C(t_c - t)^n$, where t_c, n, and C are the free parameters, we test $E(t)$ for a reasonable fit (Fig. 9) . A satisfactory fit, however, was not found, which is most likely due to the atypical time evolutions of local temperature at the very high and very low mass coordinates. Restricting ourselves to the mass coordinate window m=[0.1,0.9], another attempt was made to match $E(t)$ to the proposed functional form, with success. Fit over the range $0.09 \leq t \leq 0.20$, we find the time evolution of energy to match the functional form for $n = 6.17$ (Fig. 10).

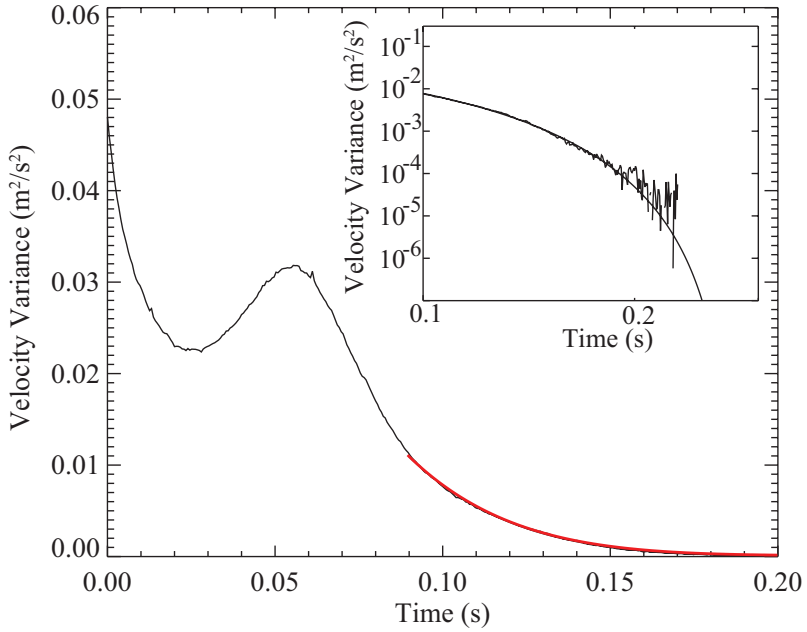

Figure 10: $E(t)$ for the mass coordinate window m=[0.1,0.9]. A non-linear fit over the range $0.09 \leq t \leq 0.20$ of the form $E = C(t_c - t)^n$ has been plotted on top of $E(t)$, where n = 6.17 was found to produce the best fit. The inset figure is a log-log plot of the same energy decay and fit.

We then proceed to make measurements of t_c in order to test the claim that collapse is simultaneous across mass coordinate [15]. Taking the strength of the power law fit (Fig. 10) to be an indication of a universal scaling behavior in $E(t)$ (the term universal is used to indicate that the scaling behavior is identical for all m), we make the assumption that $n = 6.17$ and attempt to extract t_c for all m. We divide the mass coordinate window $m = [0.1, 0.9]$ into eight smaller mass coordinate windows: $m = [0.1, 0.2], [0.2, 0.3], ...[0.8, 0.9]$. We calculate $E(t)$ for each of these windows, and we again apply the nonlinear fitting routine, leaving $n = 6.17$ fixed and keeping C and t_c as the remaining free parameters. This procedure yields to us an indirect measurement of t_c at each of the mass coordinate windows. Because t_c is not directly observable in our calculated particle trajectories (due to noise), this method of measuring t_c from a fitted function is the most reliable approach. We thus calculate eight measurements of t_c, which

correspond to eight different mass coordinate windows. To accompany these measurements, we calculate the space-time position of the collapse shock for all ten mass coordinates of width 0.1, including [0.0,0.1] and [0.9,1.0]. In Fig. 11, these measurements of the collapse time t_c and the space-time position of the collapse shock have been plotted on top of the temperature field.

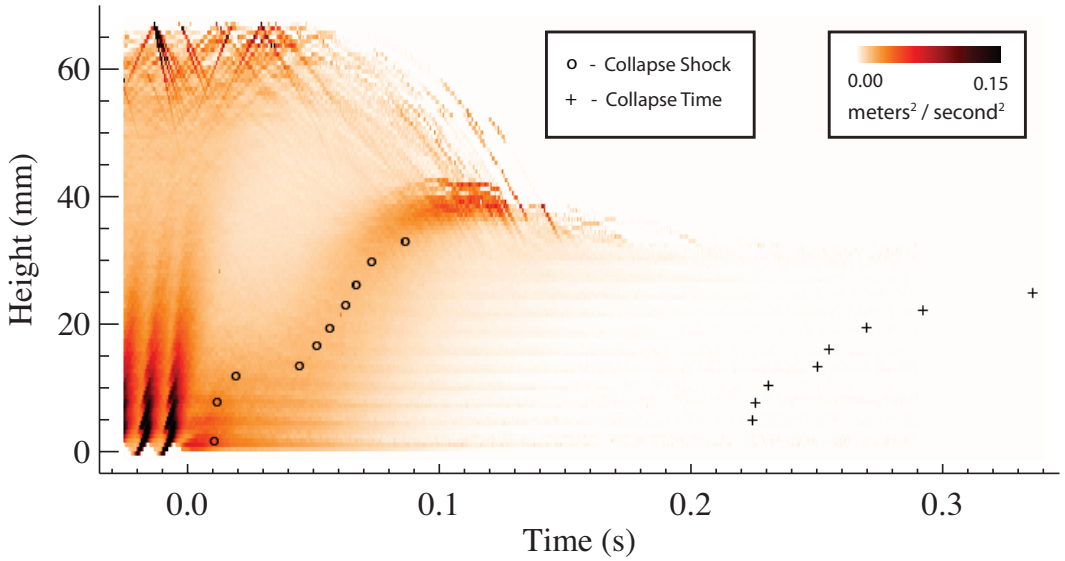

Figure 11: For mass coordinate windows of width 0.1, starting with m[0.0,0.1], the space-time position of the collapse shock has been plotted. The space-time position of t_c has similarly been plotted for these same mass coordinate windows with the exception of [0.0,0.1] and [0.9,1.0].

The temporal position has been calculated in each case by measuring the peak in $E(t)$ during the undriven phase ($t > 0$). The spatial position is then calculated by locating the "center of mass" of the density distribution at the calculated time-step. Strictly speaking, t_c does not have a spatial position, but for the purpose of visualizing the collapse, we have given each t_c a spatial position, calculated in the same manner as the spatial positions of the collapse shock. In Figure 11, we see very clearly a spatial evolution in t_c over time. Thus, contrary to [15], we do not observe a simultaneous collapse across mass coordinate.

However, this conclusion comes as a specific consequence of the assumption

that there is a universal scaling behavior in the decay of energy; this assumption has not yet been demonstrated. We thus test the assumption $n = 6.17$ by raising $E(t)$ to the fractional power $\frac{1}{6.17}$ for each of the mass coordinate windows specified above. The resulting plots are shown in Fig. 12, where deviations in the exponent of the power law are qualitatively seen by comparison with the guides provided. While $E(t)$ appears to conform fairly well to the assumed power law in some mass coordinates windows, it performs less well in the higher mass coordinate range. This suggests deviation from the assumed universal scaling behavior, and as a result, we cannot be sure how accurate the previously calculated measurements of t_c are. However, we can consider our measurements of t_c to be a first order approximation, and as we see in the following section, our fundamental conclusion that t_c is not simultaneous across m remains.

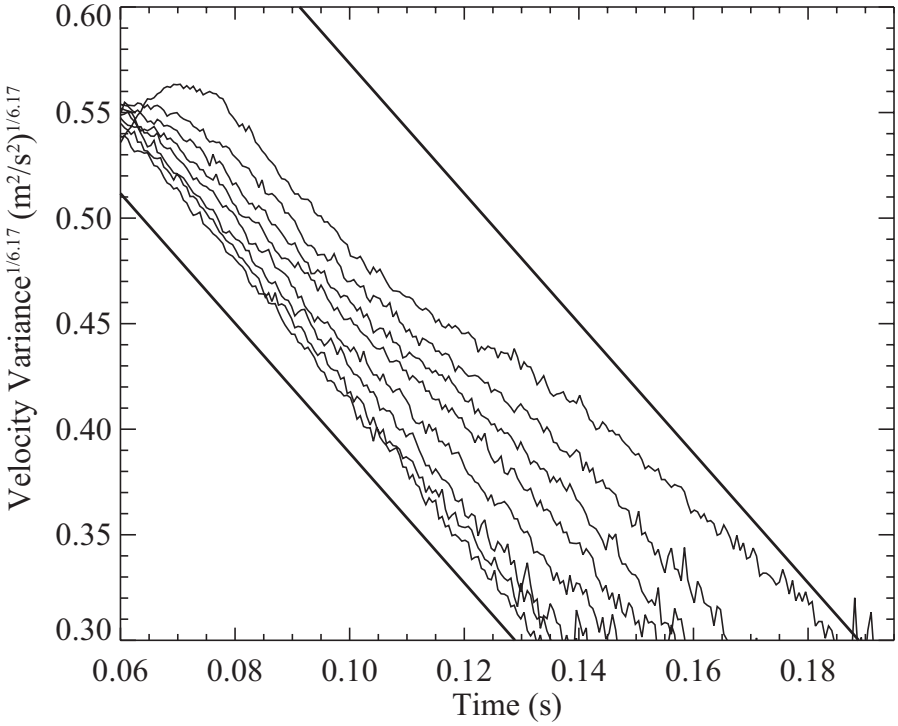

Figure 12: For mass coordinate windows [0.1,0.2],[0.2,0.3],...[0.8,0.9], E(t) raised to the fractional power $\frac{1}{6.17}$ is plotted. At both ends, the expected slope has been plotted to serve as a guide to the eye. The separation of the plots occurs naturally, and follow left-to-right, starting with $E(t)$ for $m = [0.1, 0.2]$ at the far left.

3.4 Scaling Behavior in the Local Energy, $E_m(t)$

Because measuring $E(t)$ as a global velocity variance tends to average over spatial inhomogeneities, we will continue to make use Lagrangian mass windows of width 0.1 as the range over which we calculate $E(t)$. In particular, subdividing the range of mass coordinates into 10 mass coordinate windows works well to balance between the small scale (local homogeneities) and the large scale (better statistics). Additionally, the subdivision into 10 windows mirrors the number of monolayers in the perfectly packed static state of our granular flow, which allows interpretation of the mass coordinate window to be somewhat more intuitive. In order to distinguish between the global velocity variance $E(t)$ and the velocity variance "global" only to a mass coordinate window of width 0.1, we will denote the latter $E_m(t)$.

In Fig. 13, $E_m(t)$ is plotted for four different mass coordinate windows. We will first characterize some of the general physics depicted here. Moving from lower to higher mass coordinates, the energy fluctuations of the driven granular gas ($t < 0$) lose magnitude and shift slightly in phase. In mass coordinate window $m = [0.8, 0.9]$, the energy fluctuations are seen to have largely lost their phase dependence, which reflects the homogeneity of the granular gas in this region. For $t > 0$, higher mass coordinates are observed to experience a higher temperature collapse shock. In particular, we observe that the energy in the time of the collapse shock is greater than the energy in the driving state for m=[0.8,0.9]. For the lower mass coordinates, however, the opposite hierarchy of energy is observed. In $m = [0.2, 0.3]$, no discernable collapse shock is even observable, and $E_m(t)$ is of exceptionally high magnitude during the driving stage. The absence of a collapse shock at $m = [0.2, 0.3]$ corresponds to the space-time region below regime D in Fig. 8, where the mean free path is too low for particles to freely fall, and particles are sandwiched between a falling gas above and the chamber wall below.

More significantly, Fig. 13 consolidates the claim we tentatively posited in the previous section, that t_c does not happen simultaneously over height. Following $E(t)$ out to late times, we observe temporal segregation of energy decays, in which the chronology of the collapse shock is preserved.

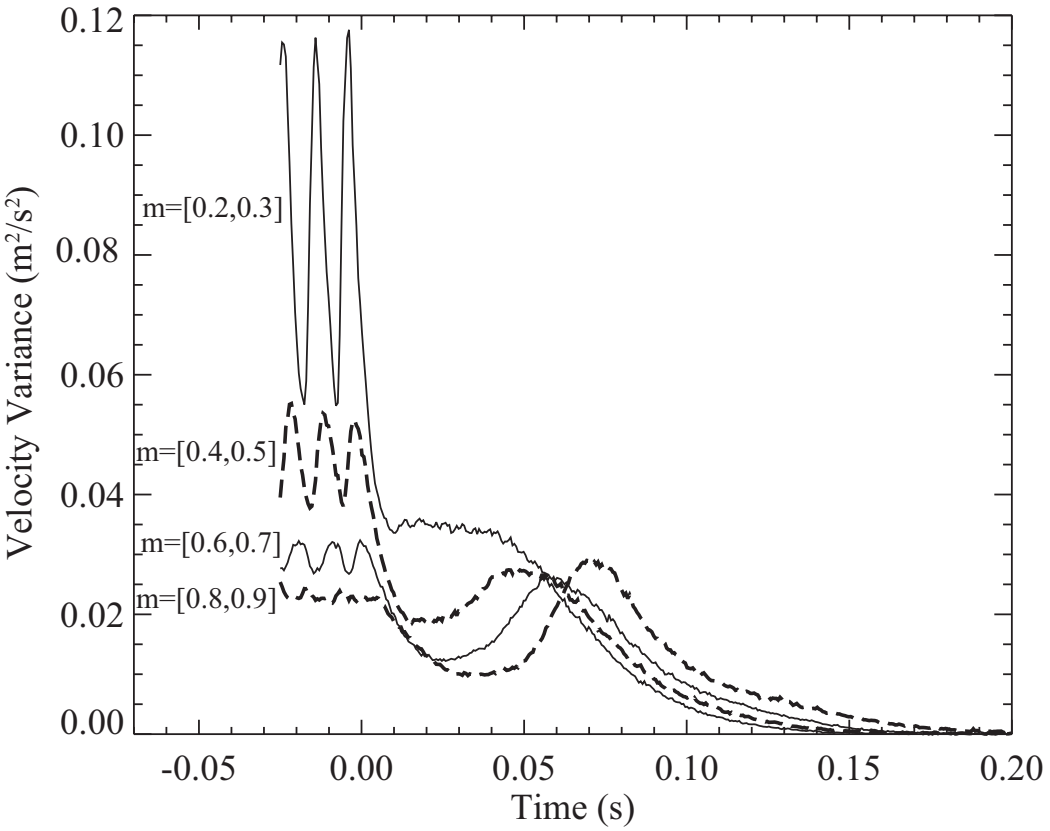

Figure 13: Energy calculated on mass coordinate windows [0.2-0.3], [0.4-0.5], [0.6-0.7], and [0.8-0.9].

The spatial inhomogeneity introduced by gravity into the inelastic collapse is thus seen in Fig. 13. With the scaling behavior predicted in the work of Volfson et al. [15] in mind, we now proceed to closely analyze our data for confirmation of such a scaling behavior in $E_m(t)$. In Fig. 14, $E_m(t)$, for $m = [0.2, 0.3]$, is plotted to several different fractional powers to see the plausibility of a power law decay. For $n = 2$, which is the power law exponent suggested in [15], a power law fit appears difficult for any range of t. At $n = 5$, however, a linear plot emerges.

This linearity indicates a good agreement between the tested exponent n and the actual exponent n_{actual} by a simple mathematical relation: $E(t) = (t_c - t)^{n_{actual}} \Rightarrow E^{1/n}(t) = (t_c - t)^{n_{actual}/n}$. At the more extreme exponent $n = 9$, the plots gain curvature once again, thus restricting the plausibility of a power law to the vicinity of $n = 5$. To test this observation more rigorously, we again turn to a non-linear fitting routine, using the functional form $E = C(t_c - t)^n$. The best fit was indeed found at $n = 5.121$.

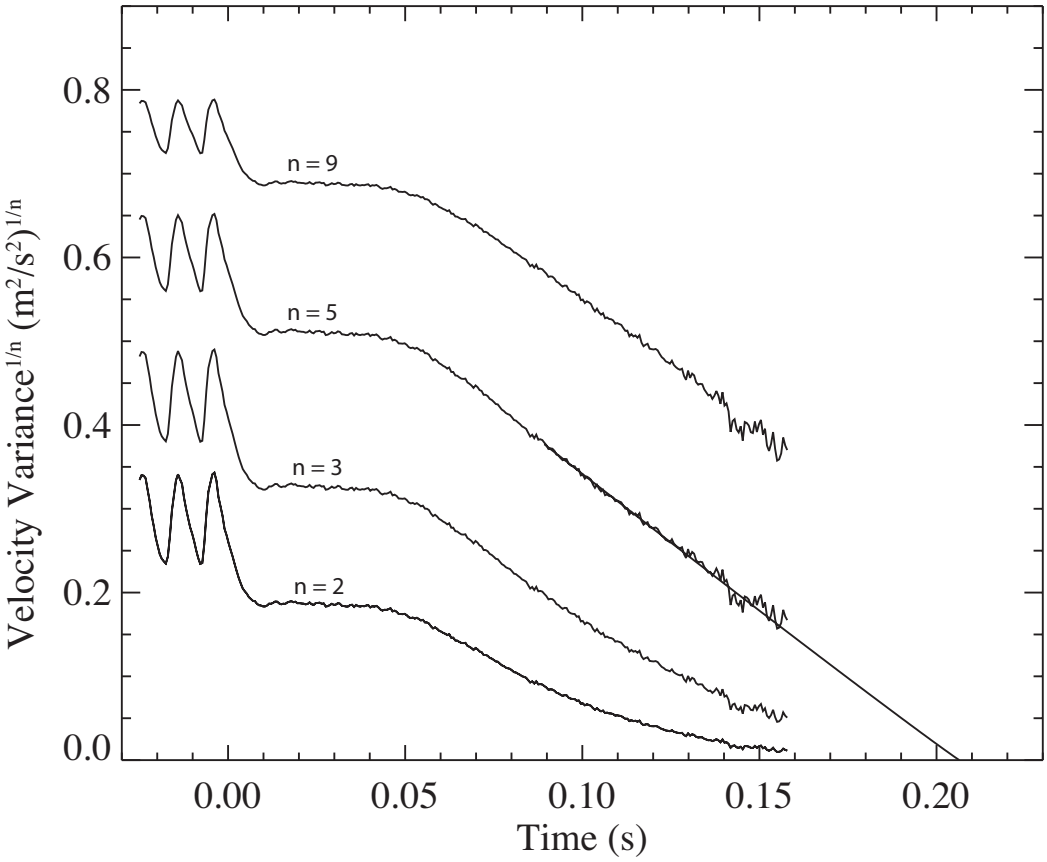

Figure 14: At mass coordinate window m=[0.2-0.3], the $E_m(t)$ of the system is taken to several fractional powers: n=2, 3, 5, and 9. The greatest linearity is observed at n=5. A nonlinear fit of functional form $E = C(t_c - t)^n$ has been plotted on top of $E(t)^{1/5}$ to demonstrate the strength of the fit. All of the plots depicted have been cut off at $t = 0.16$ due to the fact that raising E(t) to a fractional power greatly amplifies the noise in the data.

Applying the nonlinear fitting routine to the other mass coordinate windows, we find that although $E_m(t)$ exhibits a scaling behavior over all mass coordinate windows, the exponent of the power law decay is not constant and ranges over a number of values $4 \leq n \leq 7$. This result agrees well with Fig. 12, where there appeared to be some deviation in $E_m(t)$ from the power law of exponent 6.17. From these results, we conclude that while we see no evidence for a power law decay in $E_m(t)$ of the predicted exponent 2 [15], we do see evidence for a non-universal scaling behavior in $E_m(t)$, with a power law exponent in the range of 4 to 7, depending on m.

The derivation of the power 2 prediction in [15] emerged from solutions to granular hydrodynamic equations under the assumption that $\epsilon << 1, \Lambda^{-2}$, where $\epsilon = \pi^{-1/2}(\frac{width\,of\,cell\,in\,particle\,diameters}{total\,number\,of\,particles})$ and $\Lambda^2 = \frac{1-r^2}{4\epsilon^2}$. For the regime of quasi-static flow (Regime E in our discussion), the hydrodynamic equations were simplified to first order in ϵ, after which two cases were considered: $\Lambda << 1$ and $\Lambda >> 1$. In both cases, differential equations for temperature were solved with appropriate approximations and confirmed with numerical solutions. In each case, it was found that $T(m,t) = (t_c - t)^2 Q(m)$, where Q is determined by a nonlinear differential equation and is only a function of m. Because m and t are separable in this solution, their result could be integrated to $E(t) \sim (t_c - t)^2$.

In our system, $\epsilon = 5.7 * 10^{-2}$ and $\Lambda^{-2} \approx 5.3$, for a coefficient of restitution approximated at $r = 0.95$. For comparison, $\epsilon = 10^{-2}$ and $\Lambda = 0.04$ are presented in [15] as values that exhibited their proposed power law, and the coefficient of restitution they tested was $r = 0.995$. Physically, ϵ corresponds to the inverse of the number of layers that form at the end of gravitational collapse and Λ corresponds to a ratio between inelastic energy dissipation and heat dissipation. Although our ϵ value is comparable to that of their simulated system, our value of Λ does not quite satisfy the condition $\Lambda >> 1$. Our measured deviation from

the power law exponent 2 may originate in part from not satisfying this condition, but it is likely that the deviation also comes from the presence several important parameters, which distinguish our granular system from their simulated system: a velocity-dependent coefficient of restitution [17], quasi-two-dimensionality, and friction. The effects of these parameters are difficult to measure, but the presence of friction can perhaps be most easily observed in the sensitivity of our measurements of t_c to mass coordinate. The fact that we observe the bottom layers of our granular flow to crystallize before the layers above is perhaps a physically intuitive result, but it is one that is not observed in the numerical system studied in [15]. The presence of friction in our granular system makes it impossible for excited particles near the top to excite the particles down at the bottom, because the frictional interactions between the particles will dissipate that energy over a relatively short distance.

3.5 Biases in the Data

The framerate at which the image data is taken is not a physical parameter of the granular gas, but it is a potentially significant parameter in our data. At too low a framerate, densely packed particles may vibrate and collide at a higher rate than the camera's framerate. And furthermore, the camera time-averages the changes in the granular gas over the length of the exposure time. Thus, certain limits are built into our ability to fully resolve particle trajectories based on image data. The question, then, is whether our framerate is high enough to be close to this limit in accuracy. In order to observe the effects of framerate on our data, we manipulated our existing data to ignore every other time-step in order to emulate data taken at 3500 Hz. In our comparison of $E_m(t)$ for two different mass coordinate windows (Fig. 15), we observe that $E_{3500}(t) < E_{7000}(t)$ for both mass coordinate windows, but that the degree of difference has a space-time dependence. If we were to take

new data in which the spatial resolution remained constant but framerate was increased by a factor of 2 to 14,000 Hz, we would expect a similar difference in $E_m(t)$ to emerge.

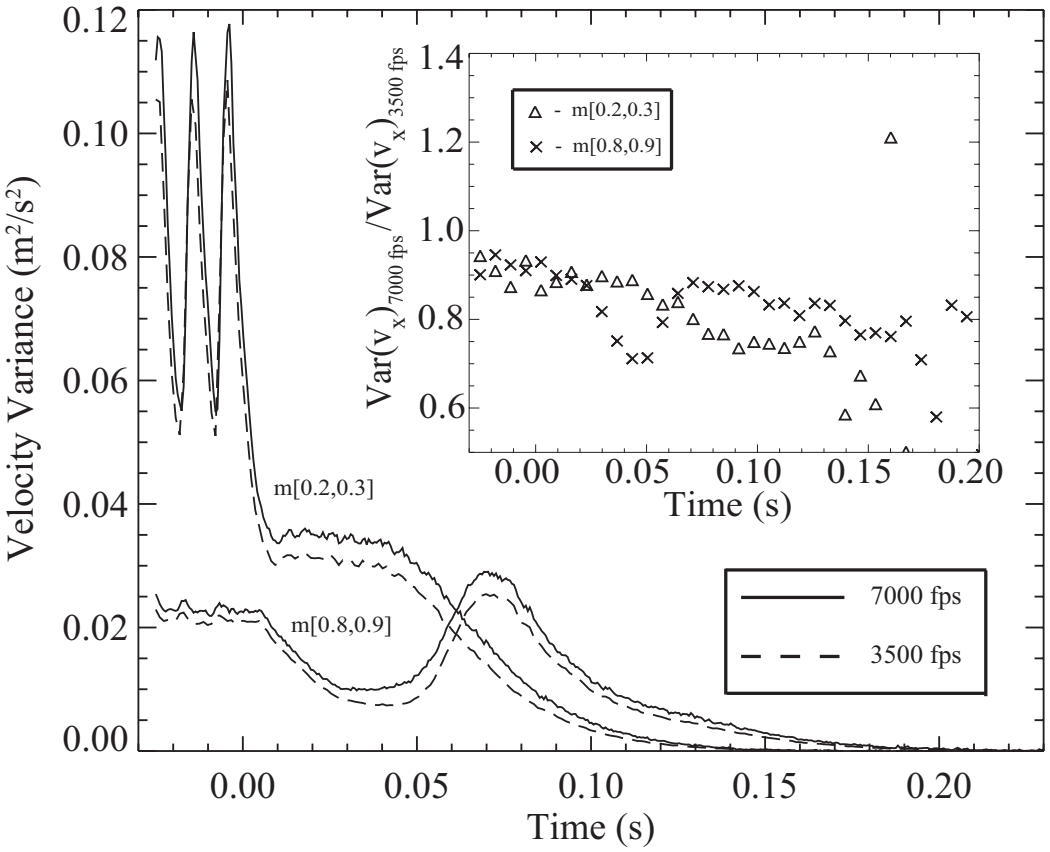

Figure 15: The effects of framerate reduction are compared for mass coordinate windows m=[0.2,0.3] and [0.8,0.9]. Inset figure: the ratio of $E(t)$ at 3500 Hz to $E(t)$ at 7000 Hz. For each mass coordinate window, agreement between $E(t)_{7000}$ and $E(t)_{3500}$ is within 15% around $t = 0$ (during the driven phase) and within 25% in the time range we fit our decay law over. As $E(t) \rightarrow 0$ for each mass coordinate, noise begins to dominate the data and agreement in $E(t)$ begins to suffer, but because this occurs far enough into collapse, we find that the power law exponents and t_c we measure remain reliable.

With regards to our power law analysis, we find the difference in the power law of the energy decay due to framerate difference to be negligible. For mass coordinate m=[0.2,0.3], the energy decay sampled at 7000 Hz gave n=7.1 while sampling at 3500 Hz gave n=6.7. For mass coordinate m=[0.8,0.9], sampling at

7000 Hz gave n=4.5 and sampling at 3500 Hz gave 4.5. These fits were done over the same fit range, and these results indicate that the temporal resolution of our energy measurements are high enough to generate accurate measurements of the exponent of the proposed power law.

4 Conclusions

In our study of the gravitational collapse of a granular gas, we have paid particular attention to the time evolution of energy close to collapse. More specifically, we have studied the vertical component of the translational kinetic energy of the particles, excluding considerations of the rotational degree of freedom available. This exclusion has been the product more of necessity than choice: it impossible to measure such quantities from 2D images. With regards to the time evolution of a granular gas through collapse, we have characterized the general phenomenology, and we have tested the existence of a theorized power law: $E(t) \sim (t_c - t)^2$ [15].

Our experimental measurements suggest that $E_m(t)$ does exhibit a scaling behavior in the late stage of a granular collapse event, but we find the scaling behavior to be non-universal across the Lagrangian mass coordinate, m. Using a nonlinear fitting routine with the functional form $E = C(t_c - t)^n$, we find that the power law exponent n ranges from 4 to 7, which indicates that our granular gas is decaying much more rapidly than in [15]. Departure from the power law proposed in [15] suggests the presence of additional parameters - such as friction [18], drag forces, and quasi-two-dimensionality - not included in their simulations and not considered in most granular hydrodynamic models. In addition to this deviation in power law exponent, our granular system exhibits an asynchronicity in the collapse time t_c across height. The fact that gravitational collapse does not happen simultaneously across all height is a significant departure from the prediction in

[15]. A number of factors are likely to contribute to these deviations, but frictional interactions are likely to be particularly responsible for the asynchronicity we observe.

References

[1] Susana Serna and Antonio Marquina. Capturing shock waves in inelastic granular gases. *Journal of Computational Physics*, 209(2):787, 2005.

[2] Kai Huang, Guoqing Miao, Peng Zhang, Yi Yun, and Rongjue Wei. Shock wave propagation in vibrofluidized granular materials. *Physical Review E*, 73(4):41302, 2006.

[3] J. Bougie, Sung Joon Moon, J.B. Swift, and Harry L. Swinney. Shocks in vertically oscillated granular layers. *Physical Review E*, 66:51301, 2002.

[4] Yaran Bromberg, Eli Livne, and Baruch Meerson. Development of a density inversion in driven granular gases. In Thorsten Pöschel and Nikolai Brilliantov, editors, *Granular Gas Dynamics*, page 251. Springer, Berlin, 1977.

[5] Rosa Ramirez, Dino Risso, and Patricio Cordero. Thermal convection in fluidized granular systems. *Physical Review Letters*, 85:1230, 2000.

[6] Klebert Feitosa and Narayanan Menon. Breakdown of energy equipartition in a 2d binary vibrated granular gas. *Physical Review Letters*, 88:198031, 2002.

[7] J. Javier Brey, M.J. Ruiz-Montero, and F. Moreno. Breakdown of energy equipartition in a 2d binary vibrated granular gas. *Physical Review E*, 63:61305, 2001.

[8] Rosa Ramírez and Rodrigo Soto. Temperature inversion in granular fluids under gravity. *Physica A*, 322:73, 2003.

[9] Peter Eshuis, Ko van der Weele, Devaraj van der Meer, Robert Bos, and Detlef Lohse. Phase diagram of vertically shaken granular matter. *Physics of Fluids*, 19(12):123301, 2007.

[10] P.K. Haff. Haff's law. *Journal of Fluid Mechanics*, 134:401, 1983.

[11] R. Brito and M.H. Ernst. Extension of haff's cooling law in granular flows. *Europhysics Letters*, 43:497, 1998.

[12] E. Ben-Naim and A. Zippelius. Singular energy distributions in driven and undriven granular media. *Journal of Statistical Physics*, 129:677, 2007.

[13] Francesco Paparella and Giuseppe Passoni. Absence of inelastic collapse for a 1d gas of grains with an internal degree of freedom. *Computers and Mathematics with Applications*, 55:218, 2007.

[14] S. Luding, M. Huthmann, S McNamara, and A Zippelius. Homogeneous cooling of rough, dissipative particles: Theory and simulations. *Physical Review E*, 58:3416, 1998.

[15] Dmitri Volfson, Baruch Meerson, and Lev S. Tsimring. Thermal collapse of a granular gas under gravity. *Physical Review E*, 73(6):61305, 2006.

[16] John Perez. *An experimental study of wave propagation and velocity distributions in a vertically driven time-dependent granular gas.* PhD thesis, Wesleyan University, 2006.

[17] N Brilliantov and T Pöschel. *Kinetic Theory of Granular Gases.* Oxford University Press, Oxford, 2004.

[18] J.S. van Zon, J. Kreft, Daniel I. Goldman, D. Miracle, J.B. Swift, and Harry L. Swinney. The classical granular temperature and slightly beyond. *Physical Review E*, 70:40301, 2004.